JP0450384

JAERI-Tech
2004-031

CHARACTERISTICS OF A LOW ENERGY AND HIGH FLUX COMPACT PLASMA SOURCE AND PRELIMINARY RESULTS IN STUDYING SURFACE MODIFICATION OF TUNGSTEN IRRADIATED BY THE SOURCE

March 2004

Guang-Nan LUO, Wataru SHU, Hirofumi NAKAMURA
Shigeru O'HIRA, Takumi HAYASHI and Masataka NISHI

日本原子力研究所
Japan Atomic Energy Research Institute

本レポートは，日本原子力研究所が不定期に公刊している研究報告書です。
入手の問合わせは，日本原子力研究所研究情報部研究情報課（〒319-1195　茨城県那珂郡東海村）あて，お申し越しください。なお，このほかに財団法人原子力弘済会資料センター（〒319-1195　茨城県那珂郡東海村日本原子力研究所内）で複写による実費頒布をおこなっております。

This report is issued irregularly.
Inquiries about availability of the reports should be addressed to Research Information Division, Department of Intellectual Resources, Japan Atomic Energy Research Institute, Tokai-mura, Naka-gun, Ibaraki-ken, 319-1195, Japan.

© Japan Atomic Energy Research Institute, 2004

編集兼発行　　日本原子力研究所

JAERI-Tech 2004-031

Characteristics of a Low Energy and High Flux Compact Plasma Source and Preliminary Results in Studying Surface Modification of Tungsten Irradiated by the Source

Guang-Nan LUO, Wataru SHU, Hirofumi NAKAMURA, Shigeru O'HIRA, Takumi HAYASHI and Masataka NISHI

Department of Fusion Engineering Research
(Tokai Site)
Naka Fusion Research Establishment
Japan Atomic Energy Research Institute
Tokai-mura, Naka-gun, Ibaraki-ken

(Received January 30, 2004)

A plasma source has been constructed in the Tritium Engineering Laboratory for investigating plasma-surface interactions in a tokamak like ITER. It is a compact device with a total length less than 1 m, compared to other existing facilities in the world. However, it can provide with stable plasma beams of low energy (~ 100 eV) and high flux (~ 10^{22} /m^2/s), close to the predicted edge plasma conditions near the ITER divertor. This report mainly describes its configuration and its characteristics, including influence of filament, arc discharge, magnetic field, bias voltage, and so on, on plasma beam being delivered towards the sample.

Also shown are the results of preliminary experiments of blister formation on tungsten samples irradiated by a deuterium plasma beam generated with the source. Hot-rolled powder-metallurgy tungsten samples of 0.1 mm thick were irradiated at ambient temperature using the plasma beam with ion flux ranging from 2×10^{21} to 1×10^{22} /m^2/s, fluence from 4×10^{22} to 1×10^{26} /m^2, and incident energy around 100 eV, corresponding to the negative bias applied on the samples. Blisters were formed over a critical fluence around 1×10^{23} /m^2. Blister density increased firstly to its maximum of 3.5×10^{4} /mm^2 at a fluence of about 2×10^{24} /m^2, and then decreased with increasing the fluence to its maximum in this work. In contrast, blister size increased monotonically up to 6 μm in diameter with the fluence till its maximum.

The results confirmed the applicability of this plasma source in simulating the ITER divertor plasma. Using this plasma source and the thermal desorption spectroscopy under construction, study on the retention of hydrogen isotopes in the plasma facing components is planned.

Keywords: Plasma Source, Plasma-surface Interactions, Nuclear Fusion

低エネルギー・高フラックスの小型プラズマ源の特性及びタングステン照射予備実験結果

日本原子力研究所那珂研究所核融合工学部
羅 廣南・洲 亘・中村 博文・大平 茂・林 巧・西 正孝

(2004年1月30日受理)

トリチウム工学研究室では、トカマクのプラズマー表面相互作用を模擬することを目的として小型プラズマ源装置を製作した。この装置は、小型(全長1m)であるにもかかわらず、ITERダイバータの周辺プラズマに相当する低エネルギー(100 eV以下)・高フラックス(約10^{22}/m^2s)のプラズマビームを生成できる特徴をもつ装置である。本報告は、その装置の構成と特性、具体的にはフィラメント、アーク放電、磁場、バイアスなどによるプラズマビームへの影響について議論する。

また、本装置を用い、タングステンを試料として予備的な照射試験を実施した。焼結後熱圧延したタングステン試料片(0.1 mm厚)に、イオンフラックス2×10^{21}~1×10^{22} /m^2/s、フルエンス4×10^{22}~1×10^{26} /m^2、エネルギー100 eV前後のプラズマビームを照射させて、表面のブリスタリング現象を調べた。1×10^{23} /m^2の閾値以上のフルエンスでは、試料表面にブリスタが観測された。ブリスタの密度はフルエンスの増加とともにはじめは増加するが、2×10^{24} /m^2のフルエンスで最大値の3.5×10^{4} /mm^2に達した後、減少していく。一方、ブリスタの大きさは単調に増加し、本試験の最大のフルエンスで直径6 μmまで成長した。

上記の結果より、本装置がITERダイバータの周辺プラズマを十分模擬できることを確認した。今後、本装置による照射実験と昇温脱離実験を組み合わせ、プラズマ対向壁における水素同位体のリテンションの研究を進める。

那珂研究所 (東海駐在):〒319-1195 茨城県那珂郡東海村白方白根2-4

Contents

目次

1. Introduction

In the presently operating fusion devices as well as future power reactors, plasma-facing materials (PFMs) are subjected to high-flux particle bombardment, including ions, neutral particles, and neutrons. In the current design of the ITER, for example, the flux and average energy of the ions and neutral particles bombarding the divertor are estimated to be $<10^{23}$ particles/m^2/s and <100 eV, respectively [1,2].

The conditions in a tokamak are nearly unique. Therefore it is best to study plasma-surface interaction (PSI) processes within the tokamak itself. However there are some substantial practical difficulties like inadequate diagnosis of local conditions (surfaces, fluxes, particle energies) because of hardness of accessibility (large and complicated vacuum vessel) and suitability (detectors would not survive the exposure for long due to plasma bombardment and high heat load). Consequently, one has to resort to complementary and alternative methods that can simulate the plasma-surface conditions of a tokamak under control. This can be realized to some extent by ion implantation experiments using either accelerators or plasma generators [3]. Accelerator-based experiments have well-defined ion energies and fluxes. The available energies and fluxes are about 0.1 keV~MeV and $<10^{20}$ ions/m^2/s, whereas plasma generator machines can yield fluxes of the order of up to 10^{22} ions/m^2/s with ion energies between 1 eV and some 100 eV, depending on the biasing of the target plate. It goes without saying that plasma generator-based experiments can produce conditions to simulate the divertor and the first wall processes.

In this report, presented are the construction of a plasma source capable of delivering plasma beams within the ranges of low energies (<100 eV) and high fluxes (~10^{22} /m^2/s), comparable to a practical edge plasma, and the preliminary results of surface modification of tungsten irradiated with the plasma source. The source is to be employed in studying hydrogen isotopes retention and migration in plasma facing components, so as to better understand one of the inevitable issues in the design of in-vessel components in a tokamak.

2. Configuration of the plasma source

The schematic view of the plasma source developed and used in this work is shown in Fig. 1. It consists of vacuum chamber and pumping, cooling, gas inlet, power supply, plasma generation, plasma delivery, sample holder, and plasma diagnosis systems. The overall configuration of the device is also shown in Fig. 2. The source is characterized by its direct-heating dual spiral LaB_6 filament and compact magnetic confinement. The former allows sufficient emission of thermal electrons at relatively low temperatures to ignite and sustain dense arc discharge plasmas from which high flux can be achieved. The latter allows easy control of beam size and density. Low energy irradiation is achieved by adjusting the negative bias voltage applied to a sample.

2.1. Vacuum chamber, cooling, and gas admittance

The vacuum chamber is roughly separated into three sections by a ceramic-metal-sealed insulation ring and a gate valve (GV1), i.e., plasma generation, transport, and irradiation sections (Figs. 1 & 2). The former two sections are always kept under good vacuum condition (10^{-6} Pa), even while changing a sample on the holder, by closing the GV1 and the GV2 and opening the AV1 (an angle valve). The pumping system consists of a turbo molecular pump (TMP, 300 l/s) and a scroll pump (SP, 250 l/min). The pressures of the sections separated by the GV1 are monitored with two ionization gauges, respectively. And the achievable background pressure is less than 5×10^{-6} Pa. All sections are earthed in the experiments, and the plasma beam energy is controlled by applying a negative bias voltage to the sample. Plasma beam size is limited first by the narrowest portion (~ ϕ 50 mm) of the chamber around the insulation ring and then is adjusted via changing the magnetic field configuration induced by coils C1, C2, and C3.

A cooling system was set up to protect the filament assembly of the plasma source and the three coils from overheating, to control temperature of the sample holder under irradiation of the plasma beam. And thermocouples (type K) were laid at six key locations, including the back of sample, the back flange of the plasma source, and so on, to monitor or to control temperatures there.

A stable gas inlet system is crucial to achieve stable plasma so that irradiation flux and fluence may be controlled steadily and easily. An mass flow controller (MFC), together with a needle valve and a stopping valve, has assured stable pressures around the working pressure of 1.5 Pa, which is quite important because the ionization gauges can not work properly under the circumstances of the strong magnetic field generated by the coils and the existence of the plasma.

2.2. Plasma generation and delivery

Plasma is ignited by an electron-emitting filament and maintained by an arc discharge power supply applied between the filament (cathode) and the grounded chamber wall (anode), being assisted by the confinement coils (C1~C3). The filament is made of LaB_6, being shaped into dual-spiral as shown in Fig. 3. It is heated directly with a low voltage and high current power supply. Thermal electrons emitted from the filament move towards the wall helically along the magnetic-curves, which enhances the collision probability of the electrons with the gas molecules being introduced into the chamber. Deuterium plasma can then be ignited under suitable conditions, say, filament current of about 60 A and arc voltage of about 60 V.

The coils (C1~C3) are not only necessary to the transport of the plasma onto the sample holder, but also helpful to the plasma ignition. They can be employed to confine the plasma into a beam and to control the beam size so that different fluxes can be obtained easily. The magnetic field generated by the coils is depicted in Figs. 4 & 5.

2.3. Sample holder and nearby plasma diagnosis

The sample holder is isolated from the grounded chamber wall so that the sample can be negatively biased to adjust the energy of ions impinging onto the sample. An isolated sheathed thermocouple is employed here to monitor the sample temperature via closely touching the backside of the sample. The purified cooling water flows through the embedded channel inside the sample holder to cool the sample (Fig. 1). The water after purification ensures enough insulation of the sample holder from the surroundings. The initial design of the sample holder is shown in Fig. 6, for holding large samples of ϕ 50 mm and 7 mm thick, with an irradiation area of ϕ 40 mm. To hold smaller samples with an irradiation area of ϕ 10 mm, a simple adapter plate was prepared with a centered hole of ϕ 10 mm, as shown in Fig. 7.

Plasma diagnosis system includes a classical single Langmuir probe through which basic plasma parameters can be measured, and a movable plane flux probe that provides us with indirect measurement of ion flux towards sample. Fig. 8, a picture taken after removing the sample holder, shows the two probes inside the irradiation chamber, both locating about 3 cm upstream away from the sample holder. The probing tip of the Langmuir probe (the right one) is made of a piece of cylindrical tungsten of ϕ 2.5 by 2.5 mm, being connected to an isolated linear motion mechanism via a ceramic-covered conducting wire. C-V characteristic is recorded and then plasma parameters can be deduced from the recorded C-V curves, according to the process described in [4,5].

Although a Langmuir probe may acquire space distribution of plasma parameters, the deduction of the plasma parameters is feasible only when the plasma has Maxwell distribution for the electron energies and negligible influence by the external magnetic field. More important parameter in irradiation experiments is ion flux incident upon a sample that may be obtained indirectly via integrating the recorded probe current over the sample area in the case of Langmuir probe. Taking it into account that strong magnetic field is always applied to ignite and adjust the plasma, which complicates greatly the measurement via the Langmuir probe, it is consequently expected to establish a flux probe to directly acquire more reliable results. Such a probe, as shown in Fig. 9 in detail and Fig. 8 in practical situation (the left one), has been prepared and works well for not so high flux (to avoid thermal electron emission due to overheating the sensor).

The probe consists of a sensor made of Mo, a disk made of Mo, insulation parts (filled by oblique lines in the figure) made of Macor (a kind of machinable ceramic), and supporting parts made of stainless steel. The sensor of ϕ 1 cm is used to collect ions. The diameter is equal or close to the normally used sample size around ϕ 1 cm. For larger samples, measurement of lateral flux distribution is necessary to obtain the total fluxes on the sample. The disk was biased to the same potential to try to simulate the environment around the practical sample on the holder for small fluxes. For larger fluxes, the disk was floating to reduce the incoming heat flow so that the sensor could work correctly.

3. Characteristics of the plasma source

3.1. Discharge characteristics

Discharge characteristic at different D_2 working pressures is shown in Fig. 10, under filament current of 55 A, and coil currents of 30 A (C1), 25 A (C2), and 25 A (C3). The results indicate that the arc voltage did not change significantly under each pressure till the maximum arc current of 24 A tested here after the discharge was ignited. It is a feature of non-self sustaining arcs that keep the voltage almost constant as the current increases till the current becomes larger than the emission current from the filament [6]. For a fixed arc current, the arc voltage increases significantly with decreasing the pressure, which results probably from a changing process of the probability of collisions between electrons and neutral particles within the plasma generation section. With decreasing the pressure, the probability decreases, and as a result, the arc current decreases, which however may be compensated by raising the discharge voltage since a larger voltage simply increases the energies of the ionized particles, in turn, enhances the collision and recover the arc current.

Discharge behavior with changing the C1 current is shown in Fig. 11. The C1 is a coil nearest to the plasma source whose function is to assist plasma ignition and to be a part of the beam delivery system. The peak magnetic flux densities generated at the C1 coil center (top of the filament) by the C1 currents of 20 and 40 A are 0.012 and 0.023 T, respectively, when the other two coils work both at 25 A. As shown in the figure, increase in the coil current results in increase in the arc voltage for a designated arc current. A magnetic field is helpful to ignite plasma since electrons are tied along the magnetic field lines, which makes the traveling path of the electrons expand and increase possibility of collisions between electrons and neutral particles. However, too strong field may impose strong confinement to the electrons in plasma, hindering their transverse diffusion towards anode [7]. In this case, increase in the arc voltage may compensate these processes and helpful to maintain a constant arc current.

It should be noted here that measurement of the working pressure is affected severely during operation of the plasma source due to the magnetic field induced by the coils and the plasma itself. Therefore, the working pressure was always measured and decided before switching the coils on, and expected not to change significantly during the operation. Limited pressure rises less than 10% were observed after the operation due mainly to plasma induced effects, e.g., impingement on and thermal desorption from the wall.

3.2. Effect of bias voltage and working pressure on holder current

To monitor current flowing onto an isolated sample holder is a convenient and useful way in discussing various effects of the influx toward a sample. Furthermore, the holder current is an in-situ parameter from which the influx may be estimated during irradiation. Fig. 12 presents a good example for one of these effects, i.e., holder current as a function of holder bias and arc current. It can be seen clearly that for any

one of arc currents tested here the holder current increased with increasing the negative holder bias till -100 V, and then reached a saturation value. The saturation level increased with the arc current. The behavior can be explained as follows. Before applying a negative bias to the holder, both electrons and ions in plasma contribute to the influx. With increasing the negative bias, the electrons are subjected to a retarding field, whereas the ions are attracted towards the holder. When only the ions constitute the influx with further increasing the negative bias, a saturation level of the holder current is achieved. In our case, the ion saturation currents are reached for any arc currents at the same bias of about -100 V that may be called ion saturation voltage. The fact that the ion saturation voltage is nearly independent of the arc current may stem from the stable arc voltage feature as depicted in Figs. 10 & 11, since the saturation voltage is determined possibly by the energies of electrons and ions, whereas the energies are dependent closely on the discharge process parameters, especially the arc voltage. And the increase in the saturation current with the arc current may be attributed simply to an increase in the plasma density.

Fig. 13 shows the variation of holder temperature with holder bias and arc current. The curves all reveal minima around a bias of -40 V, and then the temperature increases with further increasing the negative bias. In addition, the temperature always increases with the arc current for a fixed holder bias. The second feature of monotonic increase of temperature with arc current is due to increase in plasma density, in turn increase in the influx. To explain the first feature, let us review first the phenomena around a biased conducting surface in a plasma. Before applying a bias, an isolated surface is at a floating potential more negative than the plasma potential due to gathering of the electrons from the plasma so that the surface repels part of the electrons, and the total influx of two signs becomes zero eventually. When applying a negative bias to the surface, more electrons are repelled from, and more ions are attracted towards the surface. As we know, in general, energies of electrons are much greater than those of ions in low pressure plasmas. And since motion of electrons is more sensitive to any change in electric field than that of ions, the electrons repelled are much more than the ions attracted. These two points, i.e., greater energies and more repelled for the electrons, led to the decrease in temperature for the small negative bias in Fig. 13, due obviously to decrease in the input thermal power. The temperature then increased with continuously increasing the negative bias simply due to continuous increase in the energy and the number of the incoming ions. Therefore, the minimum temperatures appeared at the minimum input thermal powers from the influx.

Variation of the holder current as a function of the working pressure is shown in Fig. 14, under a fixed arc current of 2.6 A and a fixed bias of -110 V. The current decreased greatly with increasing the pressure. The decease in the current may be induced by an increase in collisions between particles that leads to more recombination of charged particles. Thus less ionized particles are transported to the holder. Also shown in Fig. 14 is the decrease in arc voltage with the pressure, coincident with as shown in Fig. 10.

3.3. Effect of magnetic confinement on plasma beam delivery

Plasma generated in the generation section can be transported as a beam to the irradiation section with

the magnetic confinement system, i.e., coils C1 to C3, of which C1 is also used to assist discharge ignition in the generation section, C3 to help adjust the magnitude and dimension of the beam at the final stage in the irradiation section, and C2 to maintain a smooth field distribution between the two sections.

As seen in Fig. 15, change in the current of coil C2 did not give any significant impact to the holder current, although the calculated peak magnetic flux density at the coil center changes greatly from 0.004 T to 0.024 T with increasing the current from zero to 40 A. A not so large maximum appeared around 25 A, indicating that a uniform confinement might be better for transporting the plasma beam towards the holder, taking into account the currents of 30 and 25 A for C1 and C3, respectively. Variation of the holder current with C3 current is shown in Fig. 16. The holder current increased with the C3 current till 20 A (0.013 T), then slightly decreased and eventually tended to saturate with further increasing the C3 current up to 60 A (0.034 T). The initial increase is due to enhanced confinement to the plasma so that more and more ionized particles move towards the holder. The saturation at the final stage is due to a fact that no more particles come to the holder when the beam size becomes small enough in comparison to that of the holder (ϕ70 mm) under strong enough magnetic field. The slight decrease after 20 A is a bit difficult to understand, which might be related to enhanced recombination processes of ions and electrons within a denser plasma beam confined by a stronger magnetic field. Observation on the plasma beam just in front of the holder revealed that the dense part of the beam became smaller with raising the C3 current. At the C3 current of 20 A, the dense part identified by eyes all irradiated on the holder. Fig. 17 shows a plasma beam in front of the holder under conditions of, pressure of 0.6 Pa, filament current of 55 A, coil currents of 35 A (C1), 10 A (C2), and 45 A (C3), arc current of 12 A, and holder bias of -100 V. Here the dense part of the beam is about ϕ30 mm.

3.4. Determination of plasma and beam parameters

The plasma and beam parameters have been evaluated with the Langmuir probe. Figs. 18 & 19 show the radial distribution of the ion saturation current with changing the arc current and the C3 current, respectively. It is expected that the distribution of plasma is nearly axisymmetric around the axis of chamber/holder because of the coil system. However the practical distribution deviated a little bit from this symmetry as observed clearly in Figs. 18 & 19, in particular in the case of large arc or C3 currents. The increase in the ion saturation current with the arc current within the whole measurement area was due to an increase in the plasma density, similar to what observed on the sample holder in Fig. 12. And the increase in the saturation current with the C3 current within the central area of ϕ55 mm (from the probe position of 20 mm to the center at 47.5 mm) resulted from a denser plasma core due to enhanced magnetic confinement. A distinctive feature in Figs. 18 & 19 is that there are steep changes in the ion saturation current from the center to the edge, indicating a nonuniform distribution on the holder.

A Langmuir probe characteristic curve recorded at the position of 20 mm is shown in Fig. 20, from which the electron temperature can be obtained as,

$$kT_e = e\left(\frac{d\ln I_{lp}}{dV_{lp}}\right)^{-1}, \quad (1)$$

where kT_e is the electron tepmterature in eV, I_{lp} the probe current, V_{lp} the probe bias in V, and e the elementary charge. And lp denotes Langmuir probe in the equation. The equation represents a electron temperature without magnetic field. Here the equation is employed only for approximately evaluating the electron temperature. Also shown are two insets depicting how to decide floating potential V_{fl} and plasma potential V_{pl}. Note that in the inset for getting plasma voltage, the ordinate is logarithmic. From the figure, here the kT_e, V_{fl}, and V_{pl} are decided to be 0.7 eV, 0.2V, and 1.3 V, respectively. At the center of 47.5 mm, they are 1~2 eV, -5 ~ -7 V, and -1 ~ -5 V, respectively, for the arc current ranging from 3 A to 7.8 A, and other conditions as indicated in Fig. 20. Therefore, one of the most important parameters in irradiation experiments, ion energy, can be decided to be the difference between the negative bias to sample holder and the plasma potential

$$E = e\left|V_h - V_{pl}\right|, \quad (2)$$

taking into account that ion temperatures are much smaller than electron temperatures in low pressure arc discharges [6].

Since V_{pl} is usually minus several volts at the center area, the energy is thus decided overwhelmingly by V_h if it is large enough, e.g., $E \approx 95$ eV if $V_h = -100$ V.

Another important parameter is the ion flux to a sample, which may be obtained indirectly with a Langmuir probe. However, the corresponding mathematic analysis is complicated and the issue is further complicated in the presence of the external magnetic field. The flux may also be obtained from the current collected by the whole sample holder, and an average flux on the whole holder is acquired. However, the error is large if the plasma is not uniform and a small sample is irradiated. A metallic plate with a hole is used to shape the ion beam into a desired irradiation area in ion beam implantation experiments so that the equipped Faraday cup can measure the whole shaped beam and give the precise flux over the area. However, in plasma beam irradiation experiments, non-uniform strong magnetic field applied around sample holder makes the practical irradiation area unequal to the tailored area with the plate. Due to these reasons, a more direct evaluation on the ion flux has been carried out using the flux probe shown in Figs. 8 & 9. The use of measurement results would be made to select the fluxes in the following irradiation experiments. The evaluation procedures are described as follows. The probe sensor negatively biased sufficiently collects only ions from plasma at its top and side surfaces. Due to different orientation of the two surfaces, an approximation can be made that the flux towards the top surface is double that towards the side surface. In the present case, the diameter of the top surface is 1 cm, and the height of the side surface 1 mm, giving the top and the side areas of $S_t = 7.85\times10^{-5}$ and $S_s = 3.14\times10^{-5}$ m^2, respectively. With the assumption, the average flux towards the top surface can be deduced as

$$f = \frac{I}{e(S_t + 0.5S_s)} = 6.63\times10^{22} I, \quad (3)$$

where f is the flux in ions/m^2/s, I the total collected current in A, and e elementary charge in C. A required flux can be achieved via adjusting plasma parameters so as to control the collected current. For example, to achieve an average flux of 1×10^{22} ions/m^2/s on a sample with an irradiation area of ϕ10 mm, a collected current of 0.15 A is required. Similar to the sample holder and the Langmuir probe, many plasma parameters affected the flux towards the flux probe.

The probe has shown some of characteristics similar with those of the sample holder and the Langmuir probe, e.g., increase in the probe current with increasing the arc current and the C1 current, and existence of the maximum probe current at the medium range of C2 current. However, C3 dependence of the probe is obviously different from what observed on the sample holder where the maximum occurred around 20 A as depicted in Fig. 16. Here the current increased monotonically with increasing C3 current as shown in Fig.21, corresponding well to the decrease in the mean free path transverse to the magnetic field determined by the electron Larmor radius [8]

$$\rho_e = \frac{(m_e kT_e)^{1/2}}{eB}, \tag{4}$$

where m_e is the mass of electron, and B the magnetic field strength. Thus a higher magnetic field suppresses the transport of plasma toward wall and increases the transport throughput. The effect has also been shown clearly in Fig. 22 where larger magnetic field made the plasma beam denser at and near the center.

3.5. Selection of experimental parameters

A filament current of 55 A was enough to achieve a temperature of the LaB_6 filament over 1400 °C so that it can generat thermal electron emission of about 1 A/cm^2. Typical D_2 discharge voltage was around 60~80 V for this device and the variation depended mainly on the working pressure and the C1 current. Lower pressures and larger C1 currents were helpful to achieve larger beam fluxes, which, however, raised arc voltage significantly. The arc voltage should be practically maintained low to avoid enormous sputtering of filament material. Thus a D_2 pressure of 1.5 Pa and a C1 current less than 35 A were chosen in the experiments to maintain a low arc voltage around 60 V. Flux adjustment was completed mainly by changing the arc current and C3 current. Based on the above results, an average flux of 1×10^{22} ions/m^2/s could be obtained on the sample of ϕ10 mm under the following designated conditions: D_2 working pressure of 1.5 Pa, filament current of 55 A, arc current of 12 A, holder voltage of -100 V, C1 to C3 currents of 35 A, 10 A, and 45 A, respectively. Larger fluxes can be achieved conveniently with further increasing filament current and / or arc current, or working pressure and / or C1 current at the expense of filament lifetime. Lower energies can also be achieved simply by reducing holder voltage with a difficulty of determining an exact flux.

4. The first irradiation test using tungsten samples

Although W is a candidate material as the PFM at divertor baffle area in ITER, understanding on the PSI

processes under the predicted edge plasma conditions, i.e., DT particle flux and energy of $<10^{23}$ ions/m^2/s and <100 eV, respectively, together with irradiation of neutron flux, is still very limited. Most of results regarding the interactions of hydrogen isotopes with tungsten came from the accelerator-based experiments ($\geq$100 eV, $\leq10^{20}$ /m^2/s, $\leq10^{25}$ /m^2) [9-19]. The obtained results have shown correlations between the hydrogen/tungsten interactions and the beam energy, flux, and fluence. However, the extrapolation of the results to the parameters range of the ITER divertor may be inappropriate where different origins of traps and defects and their effects on the PSI processes may be present.

Because of its unique advantages in simulating low energy and high flux plasmas, the plasma generator-based experiments have attracted more and more attention in fusion society. However, until now there have only been a few corresponding articles in the literature published within last several years. Plasma machines active in the field include the PISCES-B at UCSD with which Sze et al. [20,21] studied interactions between D plasma and tungsten with 1% lanthanide oxide and 99.95% pure tungsten foils, and Tokunaga et al. [22] with tungsten coated carbon. The TPE at LANL that was used by Causey et al. [23,24] and O'hira et al. [25] to deliver a mixed plasma beam of D and T to impinge powder metallurgy samples of 99.99% pure tungsten and tungsten with 1% lanthanide oxide. And the NAGDIS-I at Nagoya University with which Ye et al. [26] investigated surface morphology of tungsten subjected to H plasma irradiation. Their studies did reveal some interesting results, e.g., appearance of a new trap at 2.5 eV, and rapid escape of hydrogen from tungsten surface during intense bombardment leading to low retention eventually.

Bubble and blister formation in tungsten have complicated the understanding on the interactions of hydrogen isotopes with tungsten. The studies by Wang et al. [12], Haasz et al. [15], Sze et al. [20], Tokunaga et al. [22], Venhaus et al. [24], and Ye et al. [26] have demonstrated blistering in tungsten due to hydrogen isotope implantation. The blister formation and hydrogen isotope recycling through fissures in the blisters may affect the hydrogen isotope transport and trapping properties, in particular, the tritium inventory and dust generation in the ITER and the future fusion machines. It is currently necessary to strengthen the studies in this field, especially, the studies on the origin and revolution of bubbles and blisters, the hydrogen isotope retention related to bubble and blister formation, and the dependence of the formation on the plasma parameters similar to those for the predicted divertor edge plasma.

In view of the state of the art in the field and our capability of carrying out the like experiments conveniently using the newly established plasma source irradiation device, preliminary study on the tungsten surface irradiated with the plasma source has been performed to check the blister formation as a function of fluence.

4.1. Experimental

Powder-metallurgy and hot-rolled tungsten sheets of 99.95% pure and 0.1 mm thick manufactured by Rare Metallic Co., Ltd, were cut into samples with a diameter larger than 10 mm so that they could be mounted properly on the modified holder as shown in Fig. 7, with a fixed irradiation area of ϕ10 mm. The samples were used as-received without any pre-treatment prior to irradiation. The sample list and

corresponding flux and fluence are shown in Table 1. The lower flux of 2×10^{21} /m^2/s was employed for the low fluences less than 5×10^{23} /m^2 to have the irradiation times long enough to achieve stable plasma beams. This flux was generated under the following conditions: filament current of 55 A, arc current of 6 A, coil currents of C1 – 30 A, C2 – 25 A, C3 – 25 A, and holder bias of -100 V. The higher flux of 1×10^{22} /m^2/s was produced under filament current of 55 A, arc current of 12 A, coil currents of C1 – 35 A, C2 – 10 A, C3 – 45 A, and holder bias of -100 V. The irradiation energies were about 95 ~ 100 eV. The sample temperature was always kept near room temperature with the cycling purified cooling water. The working pressure of deuterium gas (99.71 mol% D_2, 0.29 mol% HD) was always set at 1.5 Pa, whereas the base pressure was kept at 10^{-6} Pa level. Surface morphology of the irradiated samples was observed using a scanning electron microscopy at a tilt angle of 45°. The counting of blisters was based on the SEM photos (×5000). Practically, the blister distribution was not absolutely uniform everywhere at this magnification. Correspondingly, the density values were obtained after averaging treatment on the data from different irradiated areas of the samples.

4.2. Results and discussion

As shown in Table 1 and Fig. 23, blisters appeared over a fluence of 1×10^{23} /m^2. The maximum size of the blisters increased monotonically with increasing the fluence to its maximum in this experiment. However, the blister density showed a maximum at the fluence around 2×10^{24} /m^2. Fig. 24 presents the photographs of the surface morphology after irradiation to different fluence levels, in which (a) showed small blisters with a sparse distribution occurred at the critical fluence around 1×10^{23} /m^2; (b) gave the image with the maximum blister density observed at the fluence of 2×10^{24} /m^2; and (c) presented the maximum blister size of 6 μm at the maximum fluence of 1×10^{26} /m^2 in the experiment. The small peelings on the surface are the same as before irradiation, which might form during manufacturing of the sheets.

The blister formation for the case of He implantation into metals was discussed intensively [27-30]. The energetic He ions can induce lattice damage and form gas bubbles in metals where the gas pressure is not in equilibrium with but much higher than the surface tension. Upon further implantation the bubbles grow by ejecting metal atoms from their lattice site (loop punching [30]). And the blisters form and grow by mechanism such as interbubble fracture [29]. Correspondingly, in the case of hydrogen, when they are implanted into the substrate, they will diffuse back to the surface or deeper into the material. The former then recombines on and desorbs from the surface, while the latter will eventually find vacancies, dislocations, and voids into which they are trapped. Then the formation and growth of bubbles and blisters may be governed by such mechanisms as loop punching and interbubble fracture.

In our experiment, blistering occurred at room temperature and flux of 2×10^{21} D^+/m^2/s after the fluence of 1×10^{23} D^+/m^2 was reached, indicating need of accumulation of D atoms in tungsten for the growth of blisters. For the similar ion energies around 100 eV and similar materials of powder metallurgy, Wang et al. [12] reported a critical fluence of 1×10^{25} D^+/m^2 at room temperature and flux of 6.25×10^{19} D^+/m^2/s;

Tokunaga et al. [22] found a critical fluence between 7.2×10^{24} and 7.5×10^{25} D^+/m^2 at temperature of 823 K and flux of 1.2×10^{22} $D^+/m^2/s$; and Ye et al. [26] observed a critical fluence of 1.4×10^{25} H^+/m^2 at temperature of 920 K and flux of 2×10^{21} $H^+/m^2/s$. Their critical fluences are two orders of magnitude higher than ours, which may be explained as follows. At room temperature, the formation and growth of bubbles and blisters should be much earlier in our case than in Wang et al's case as our flux was much larger than theirs, which sped up the accumulation of the incident atoms in the substrate, in turn the formation of blisters. With increasing irradiation temperature, the diffusion is enhanced, and more incident atoms travel deeper into the substrate. This is just why Tokunaga et al. and Ye et al. reported higher critical fluences in their studies.

The increase in blisters size with increasing the fluence reflected the growth of blisters, while existence of the maximum number density clearly indicated the evolution process by the interbubble fracture that obviously results in the growth of blisters and the decrease in number and works evidently after increase in bubble desity in a material. The above-mentioned three research groups also observed the similar phenomena, of which Wang et al. observed the samples bombarded at room temperature by 1 keV, 1.1×10^{20} $D^+/m^2/s$ to fluences of 1×10^{23} ~ 1×10^{25} D^+/m^2, and Tokunaga et al. and Ye et al. to fluences of 7.2×10^{24} ~ 3×10^{26} and 1.4×10^{25} ~ 4.7×10^{25} D^+/m^2, respectively, with other parameters the same as above.

Comparison of our results with the three research groups' also revealed that our blisters size was much smaller than theirs at the same fluence levels. In the case of Wang et al., the higher ion energy might be responsible for this since the ions with energy of 1 keV had a range of 10 nm, and were able to create new defects along their paths in tungsten, leading to enhanced diffusion and deeper trapping of the incident ions, as indicated by the ERD analysis. The deeper distribution resulted in the larger blister sizes as more bubbles formed deeper need to fuse together to obtain a high enough gas pressure to form a deeper blister. Another reason may be the shallow formation of bubbles at low energies like our cases, leading to easier permeation of deuterium from the bubbles which may be further enhanced by the higher surface temperature due to shallow implantation depth and low thermal conductivity at or near surfaces. As for the temperature factor in Tokunaga et al. and Ye et al.'s studies, it played a similar role in the issue to the higher energy due simply to the enhanced diffusion processes by raising the temperature. However, as revealed by some studies [12,26], there was no blisters formation if the sample temperature was high enough because most of traps were inactive at high temperatures. The critical temperature may depend on many factors such as material composition and intrinsic defects.

5. Conclusions

(1) A compact plasma source device for simulating tokamak edge plasma has been constructed. The energy of the ions incident onto the sample can be adjusted via changing the negative bias applied to the sample holder, while the flux up to 10^{22} $/m^2/s$ level can be achieved easily via adjusting the plasma parameters. The device is able to provide a stable plasma beam for a long time operation.

(2) Preliminary experiment of deuterium irradiation on powder metallurgy tungsten samples indicated that the blisters formed at a fluence over 1×10^{23} $/m^2$. The blister density reached its maximum of 3.5×10^4

/mm^2 at the fluence of about 2×10^{24}/m^2, and then decreased with further increasing the fluence up to its maximum of 1×10^{26}/m^2 in this work. In contrast, the blister size increased monotonically up to 6 μm in diameter with the fluence in the range tested.

Acknowledgements

The authors would like to express their sincere gratitude to Drs. Y. Okumura and K. Nakamura (JAERI), for their great contribution in the initial design of the device, and to Dr. K. Hashimoto and Mr. H. Ogata (Toshiba Corp.) for their valuable assistance in the manufacturing of the device. Special thanks are also presented to Drs. M. Seki, S. Seki, H. Takatsu and H. Tsuji (JAERI) for their encouragement and support to this work.

References

[1] Federici G., et al.: Nucl. Fusion, 41(12R), 1967 (2001).

[2] ITER Technical Basis, ITER FDR Documentation Series No. 24, IAEA, Vienna, 2002.

[3] Ehrenberg J. K., in: Physical Processes of the Interaction of Fusion Plasmas with Solids, eds. W. O. Hofer and J. Roth (Academic Press, 1996), Chapter 2.

[4] Electrical Probes for Plasma Diagnostics, Swift J. D. and Schwar M. J. R., London Iliffe Books Ltd., 1970.

[5] Principles of plasma diagnostics, Hutchinson I. H., Cambridge University Press, 1987.

[6] Gas Discharge Physics, Raizer Yuri P., Springer-Verlag, 1991.

[7] Plasma phenomena in gas discharges, Franklin Raoul N., Oxford University Press, 1976.

[8] Anders A., Anders S., and Brown Ian G.: J. Appl. Phys., 75(10), 4900 (1994).

[9] Garcia-Rosales C., Franzen P., Plank H., Roth J., and Gauthier E.: J. Nucl. Mater., 233-237, 803 (1996).

[10] Alimov V. Kh. and Scherzer B. M. U.: J. Nucl. Mater., 240, 75 (1996).

[11] Wang Wenming, Alimov V. Kh., Scherzer B. M. U., and Roth J.: J. Nucl. Mater., 241-243, 1087 (1997).

[12] Wang Wenming, Roth J., Lindig S., and Wu C. H.: J. Nucl. Mater., 299, 124 (2001).

[13] Ogorodnikova O. V., Roth J., and Mayer M.: J. Nucl. Mater., 313-316, 469 (2003).

[14] Haasz A. A., Davis J. W., Poon M., and Maccaulay-Newcombe R. G.: J. Nucl. Mater., 258-263, 889 (1998).

[15] Haasz A. A., Poon M., and Davis J. W.: J. Nucl. Mater., 266-269, 520 (1999).

[16] Poon M., Davis J. W., and Haasz A. A.: J. Nucl. Mater., 283-287, 1062 (2000).

[17] Haasz A. A., Poon M., Maccaulay-Newcombe R. G., and Davis J. W.: J. Nucl. Mater., 290-293, 85 (2001).

[18] Poon M., Maccaulay-Newcombe R. G., Davis J. W., and Haasz A. A.: J. Nucl. Mater., 307-311, 723 (2002).

[19] Causey R. A.: J. Nucl. Mater.: 300, 91 (2002).

[20] Sze Fan C., Doerner Russ P., and Luckhardt Stan: J. Nucl. Mater., 264, 89 (1999).

[21] Sze Fan C., Chousal Leo, Doerner Russ P., and Luckhardt Stan: J. Nucl. Mater., 266-269, 1212 (1999).

[22] Tokunaga K., Doerner R. P., et al.: J. Nucl. Mater., 307-311, 126 (2002).

[23] Causey R. A., Wilson K., Venhaus T., and Wampler W. R.: J. Nucl. Mater., 266-269, 467 (1999).

[24] Venhaus T., Causey R., Doerner R., and Abeln T.: J. Nucl. Mater., 290-293, 505 (2001).

[25] O'hira S., Steiner A., et al.: J. Nucl. Mater., 258-263, 990 (1998).

[26] Ye M. Y., Kanehara H., Fukuta S., Ohno N., and, Takamura S.: J. Nucl. Mater., 313-316, 72 (2003).

[27] Scherzer B. M. U., in: Sputtering by Particle Bombardment II, ed. Behrisch R. (Springer, Berlin, 1983).

[28] Picraux S. T., Vook F. L.: J. Nucl. Mater., 53(1), 246 (1974).

[29] Evens J. H.:J. Nucl. Mater., 76&77, 228 (1978).

[30] Terreault B., et al.: J. Nucl. Mater., 68, 334 (1977).

Table 1. Flux and fluence for each sample and size and density of generated blisters

Flux(/m^2/s)	2×10^{21}			1×10^{22}				
Fluence(/m^2)	4×10^{22}	1×10^{23}	2×10^{23}	5×10^{23}	2×10^{24}	1×10^{25}	2×10^{25}	1×10^{26}
Irrad. time	20s	50s	1m40s	50s	3m20s	16m40s	33m20s	2h47m
Blister size(μm)	0	≤0.5	≤1	≤ 2	≤ 2.5	≤ 2	≤ 3.5	≤ 6
Blister density (10^4/mm^2)	0	Rare	1	3.2	3.5	3.2	0.95	1.4

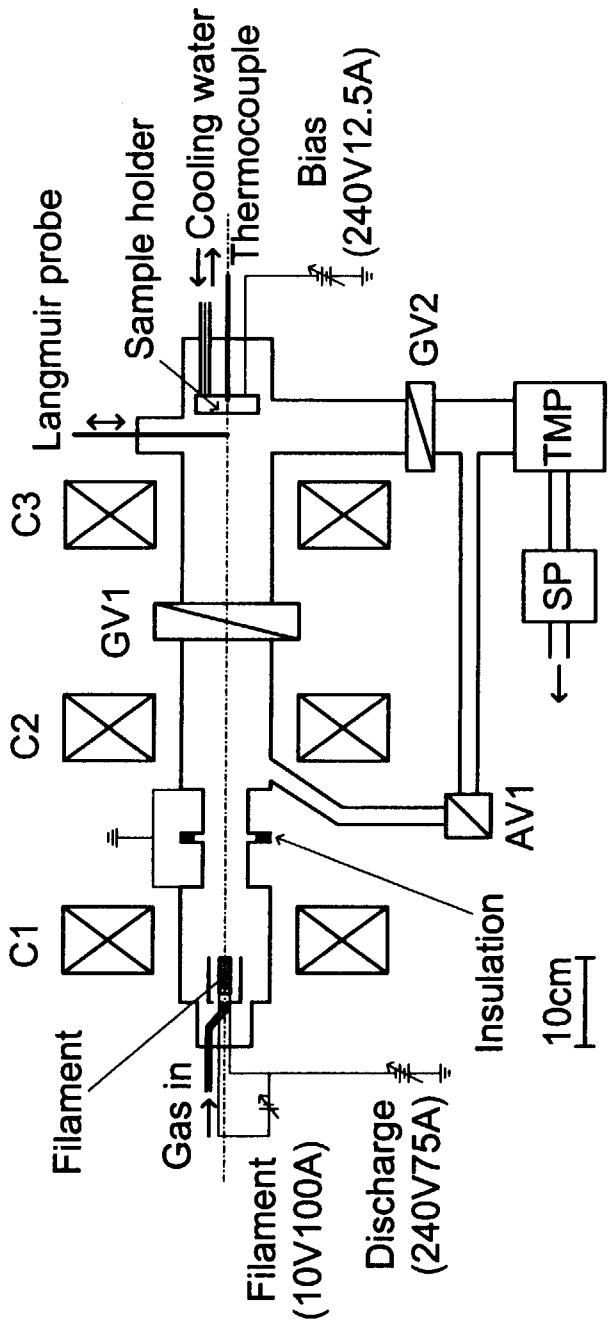

Fig. 1. Schematic figure of the compact plasma source.

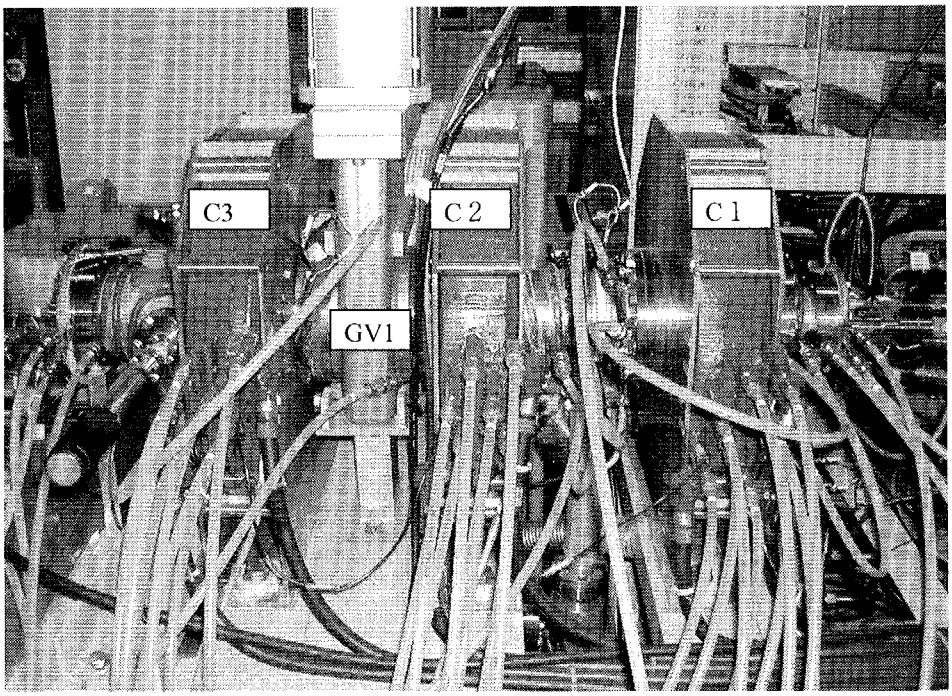

Fig. 2. A photo showing the overall configuration of the plasma souce. To the right is the plasma generation section, and to the left the irradiation one (sample holder). Total length is about 800 mm.

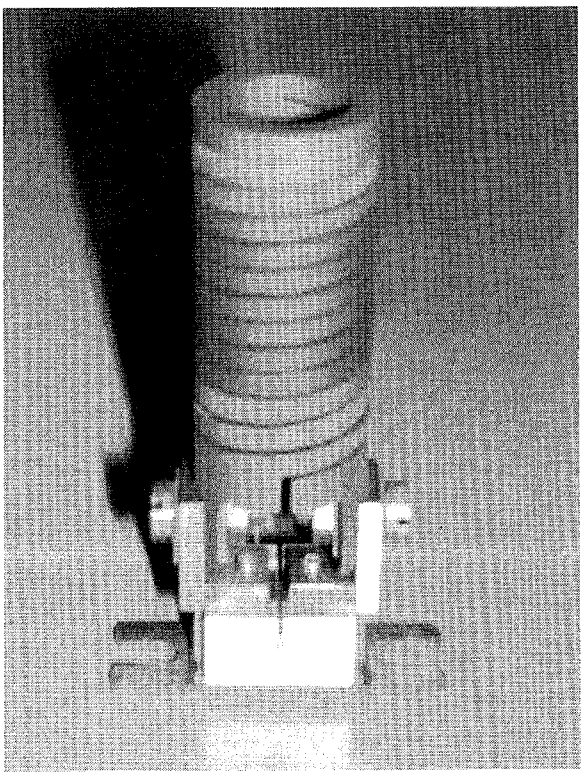

Fig. 3. Photo of dual-spiral LaB_6 filament for generating plasma. Sizes of the heating portion are external diameter of 15 mm and height of 35 mm.

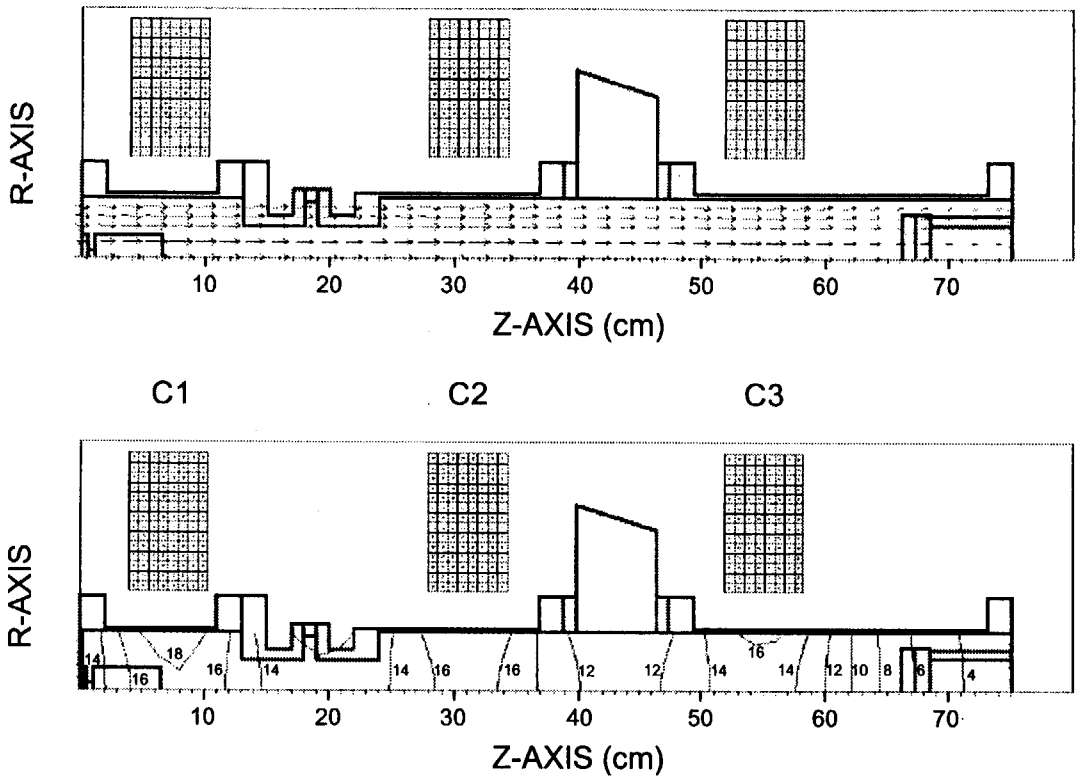

Fig. 4. Magnetic field distribution of the device, formed under currents of 30, 25, and 25 A for the three coils of C1 to C3, respectively. To the left is the plasma source, and to the right the sample holder. The upper figure shows the vector distribution of the field (strength and direction), and the lower the contour distribution. The abscissa is Z-axis along the axis of the vacuum chamber, and the ordinate R-axis (radial direction). The unit of the magnetic flux density on the contour curve is mT.

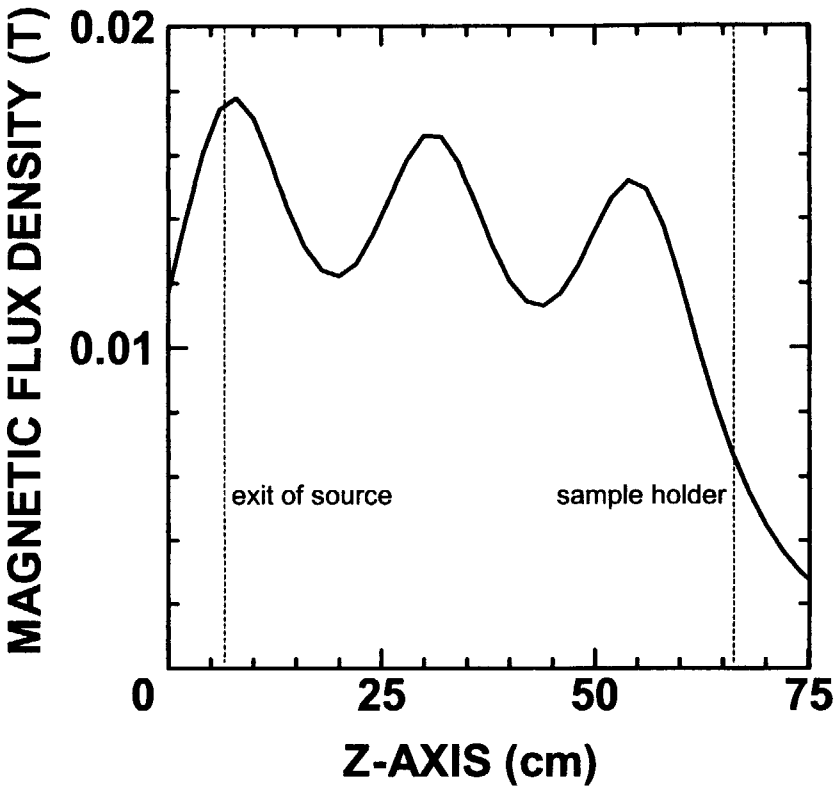

Fig. 5. Magnetic flux density along Z-axis under the same conditions as in Fig. 4, showing a field of 0.0175 T near the exit of the plasma source, and 0.007 T around the sample holder. Three peaks correspond to the central planes of the three coils (see also Fig.4).

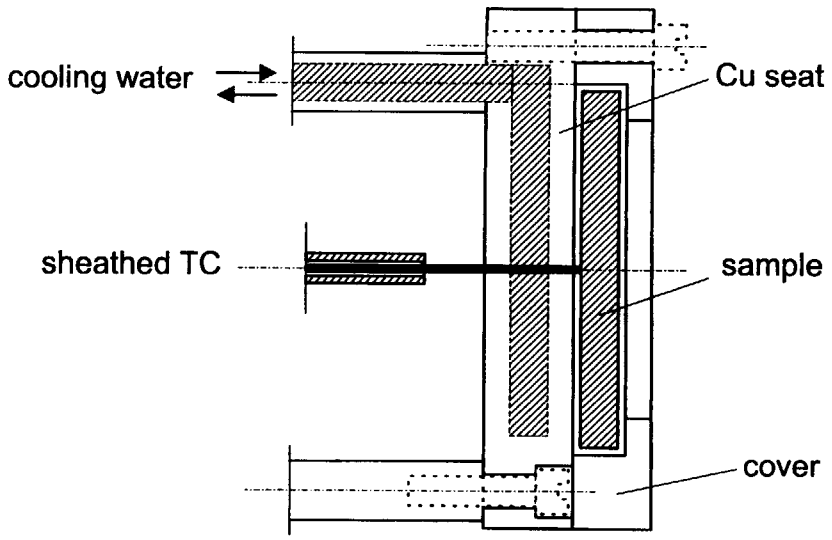

Fig. 6. The original design of the sample holder for large samples of ϕ 50 mm and 7 mm thick. The Cu seat is cooled by the purified water, and temperature is monitored via a sheathed thermocouple.

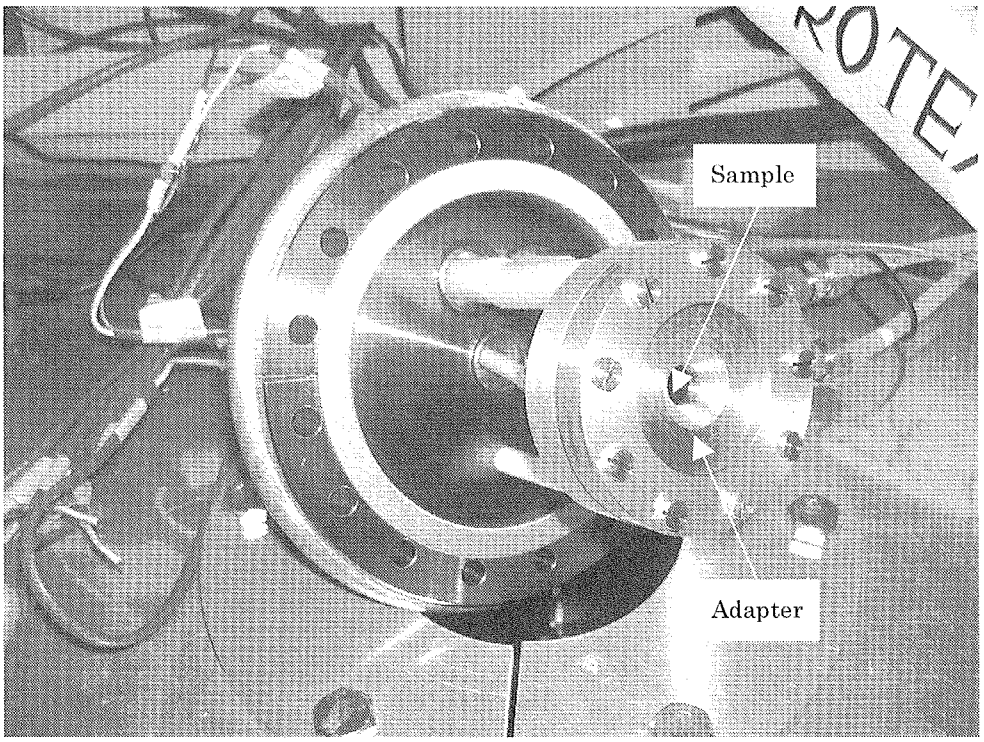

Fig. 7. Sample holder with an adapter plate for holding smaller samples, with a fixed irradiation area of ϕ 10 mm as indicated in the figure.

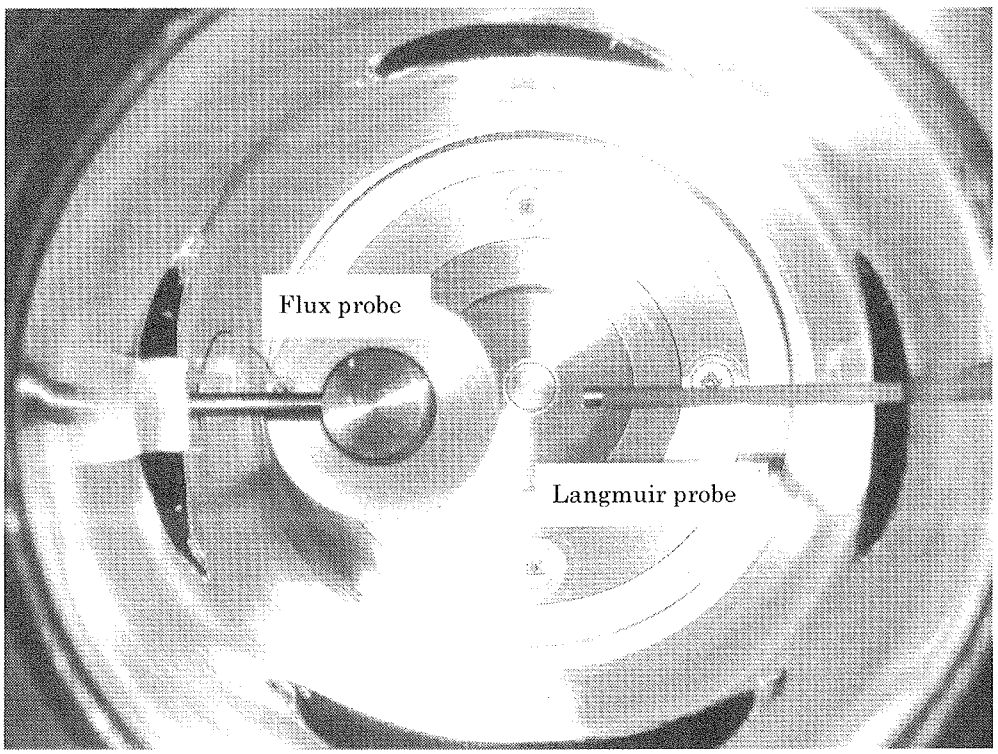

Fig. 8. A photo showing Langmuir probe with a tip of ϕ2.5 by 2.5 mm and movable flux probe (backside).

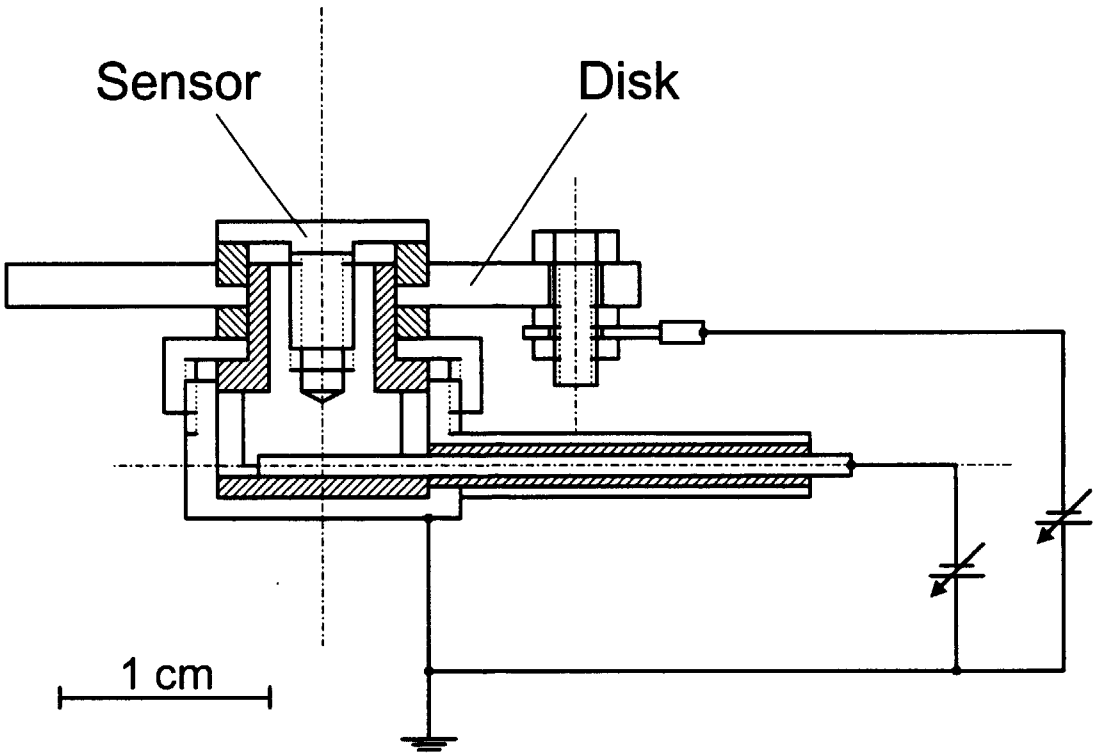

Fig. 9. Movable flux probe with a sensor whose area is comparable to the irradiated area of sample.

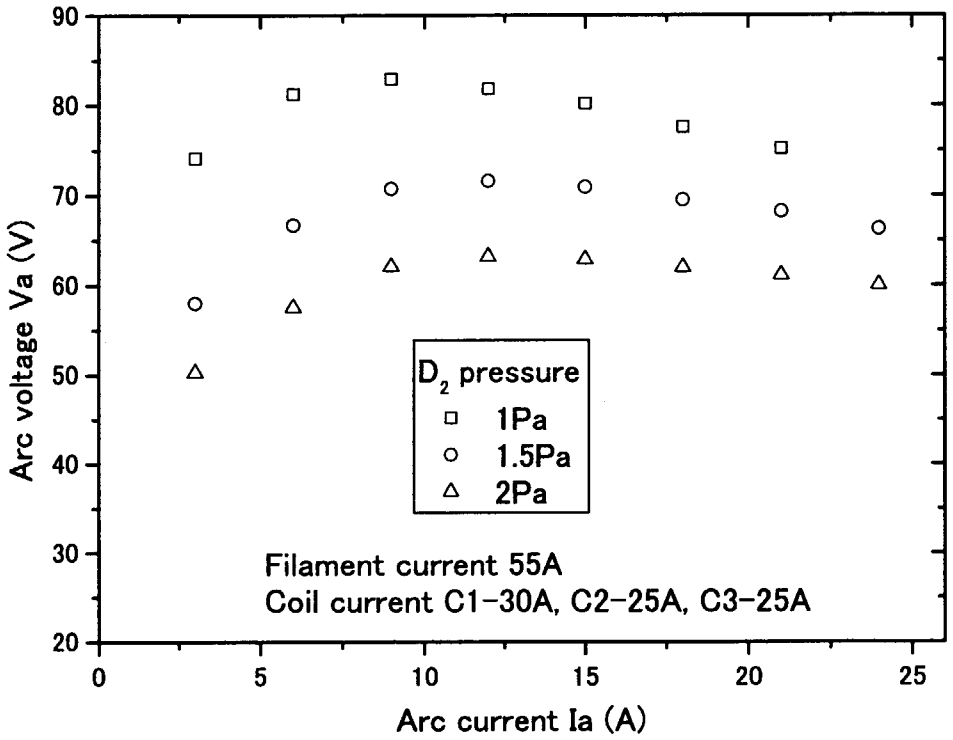

Fig. 10. Discharge characteristic of D_2 plasma at different working pressures.

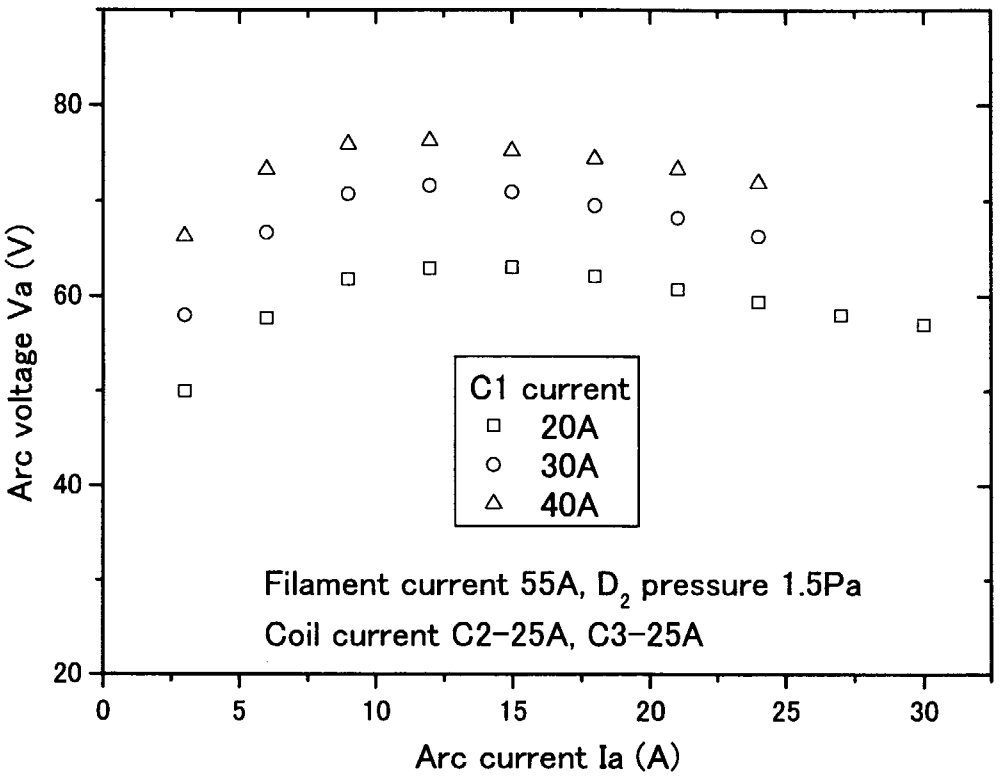

Fig. 11. Discharge characteristic of D_2 plasma at different magnetic fields generated by different currents of coil C1.

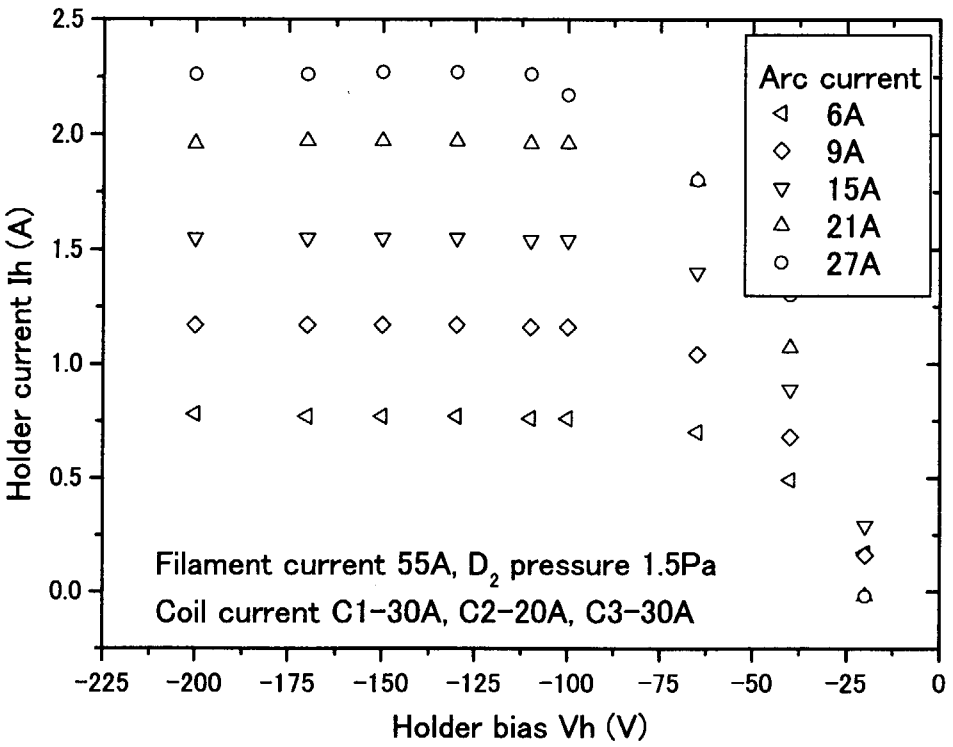

Fig. 12. Holder current Ih as a function of the holder bias Vh and arc current Ia.

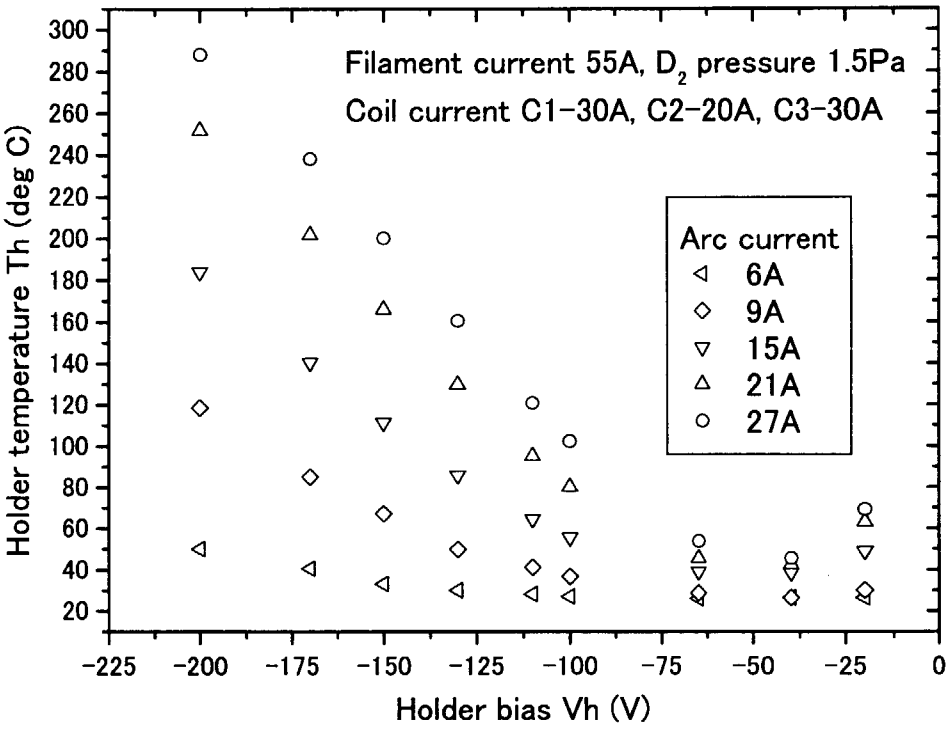

Fig. 13. Variation of sample temperature Th with the holder bias Vh and arc current Ia.

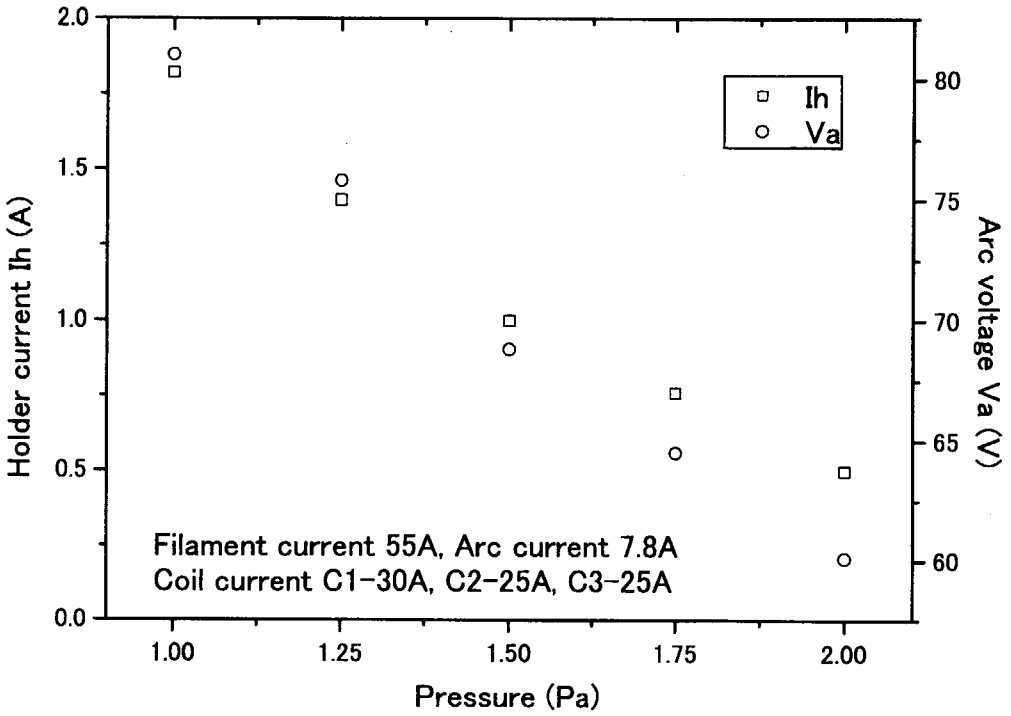

Fig. 14. Effect of working pressure on holder current Ih and arc voltage Va under a holder bias of -110 V.

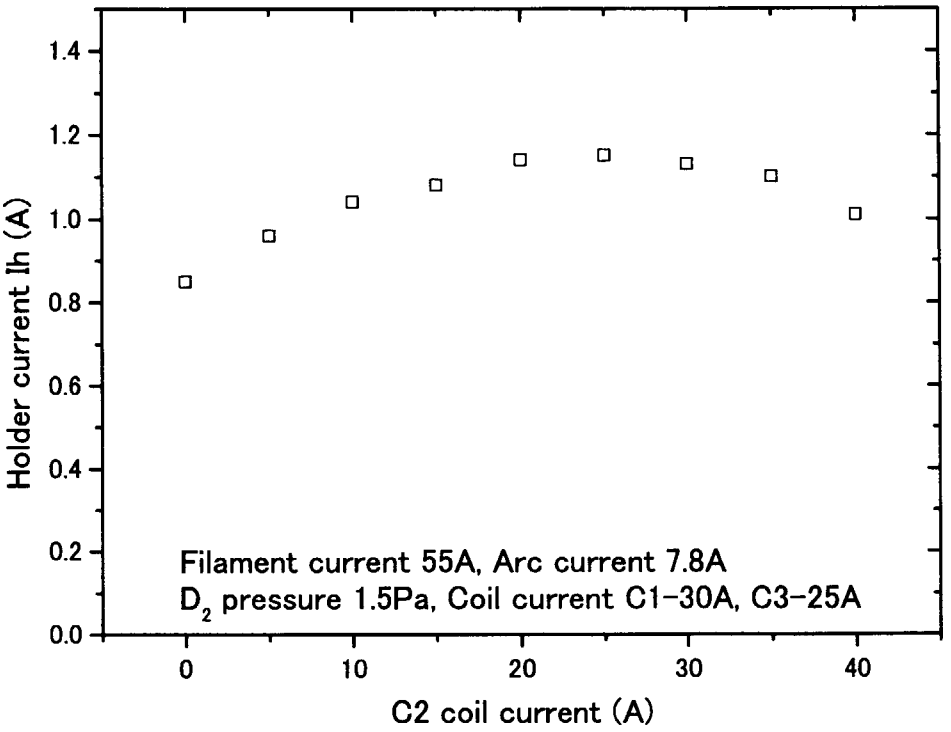

Fig. 15. C2 current dependence of transport of plasma beam to the holder biased to -110 V.

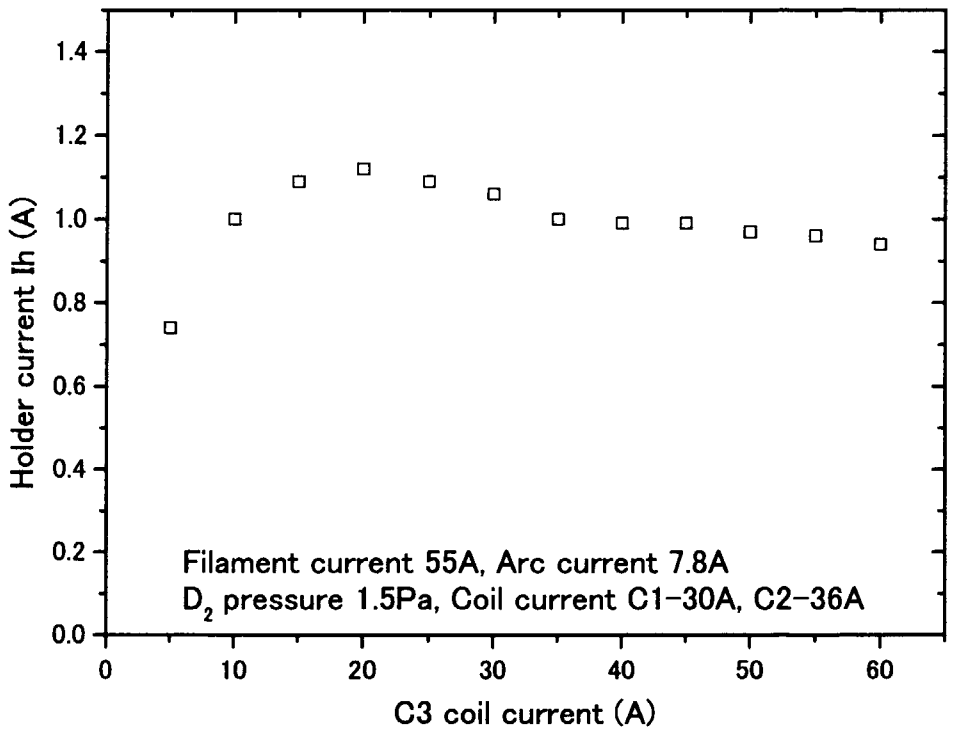

Fig. 16. C3 current dependence of transport of plasma beam to the holder biased to -110 V.

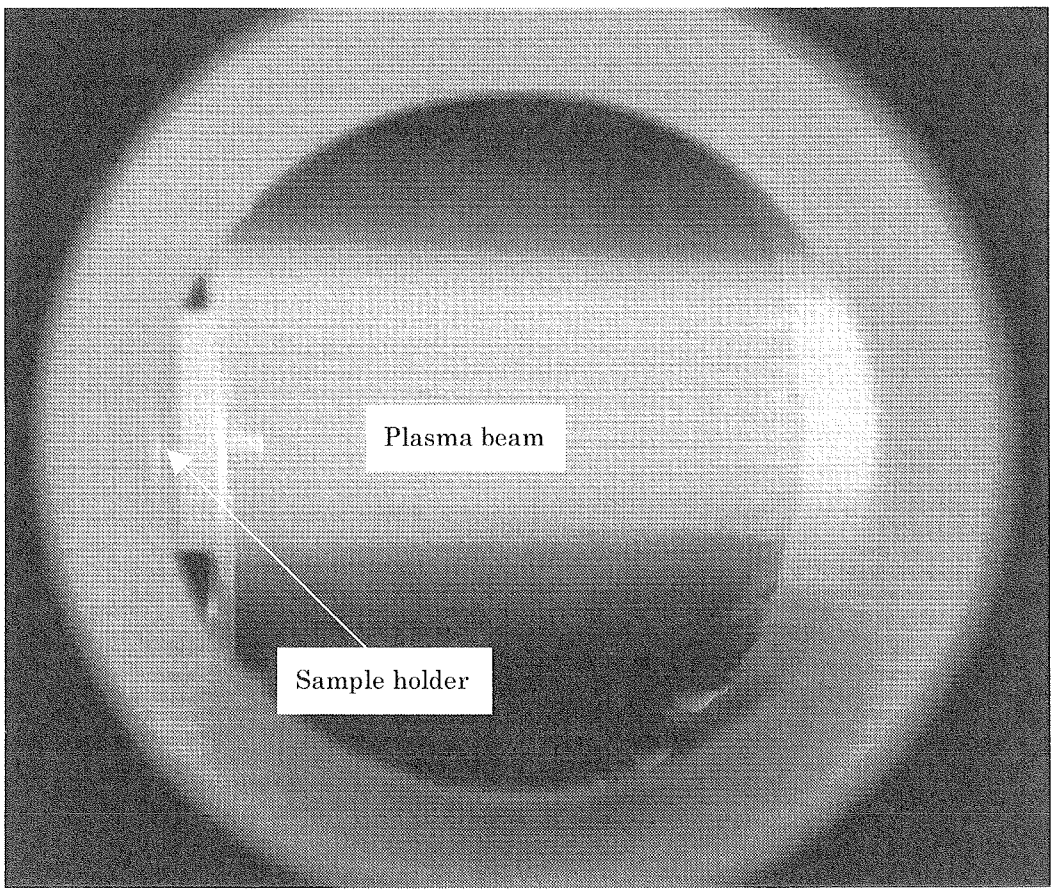

Fig. 17. A picture of the plasma beam near holder (left), with a variable size adjustable via the three coils, in particular, C3. The dense part of the beam is about 30 mm here.

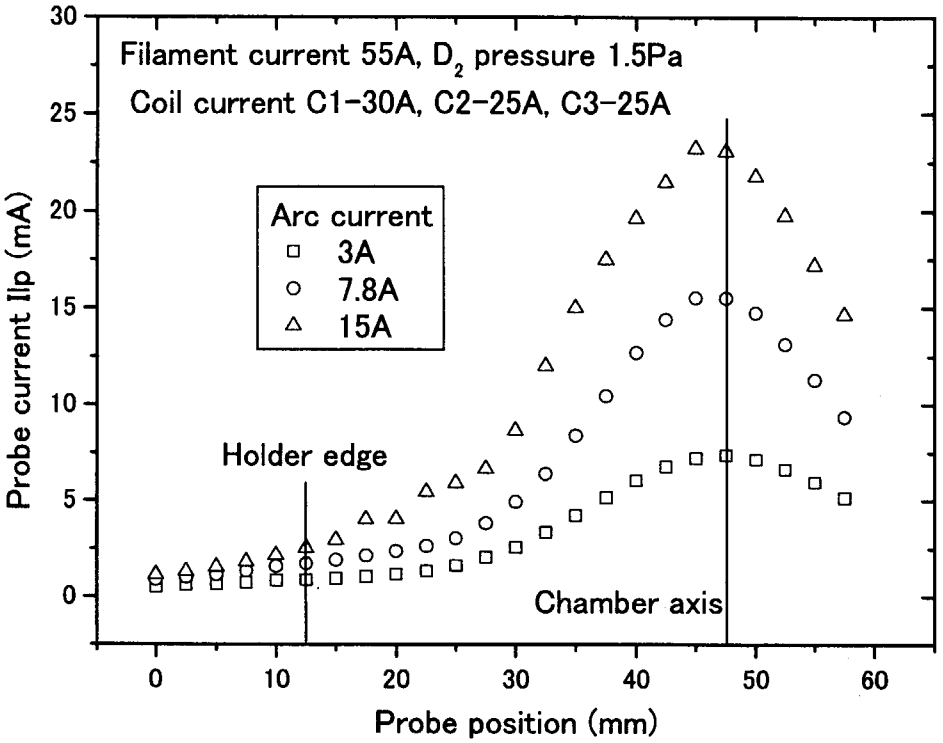

Fig. 18. Distribution of saturation ion current Ilp by Langmuir probe in front of sample holder under different arc currents, with a probe bias of -110 V.

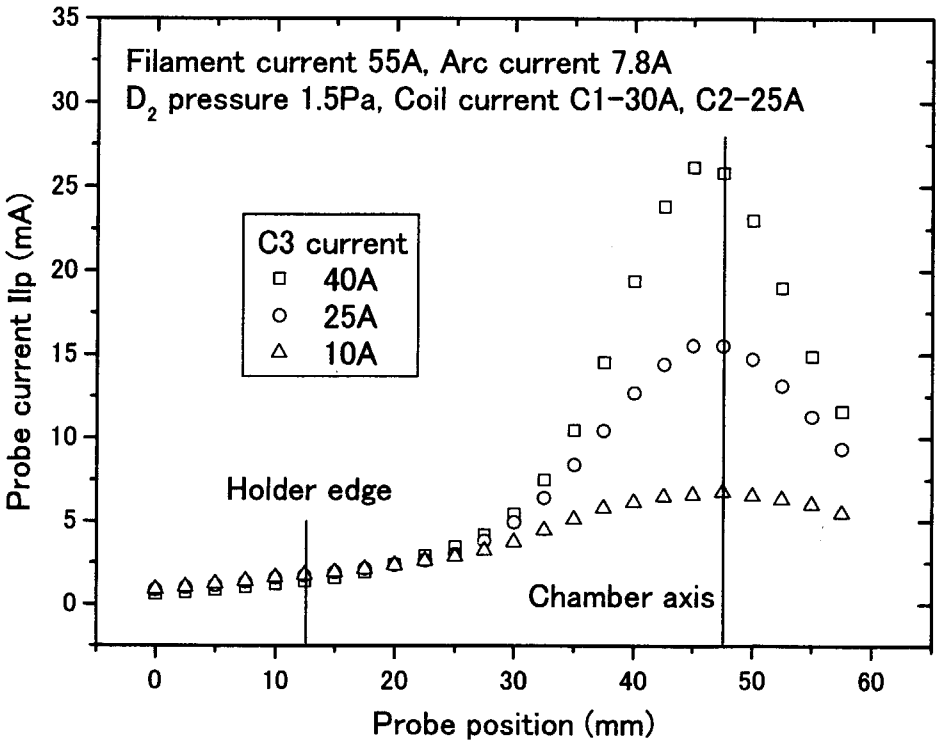

Fig. 19. Distribution of ion saturation current Ilp by Langmuir probe in front of sample holder under different C3 currents, with a probe bias of -110 V.

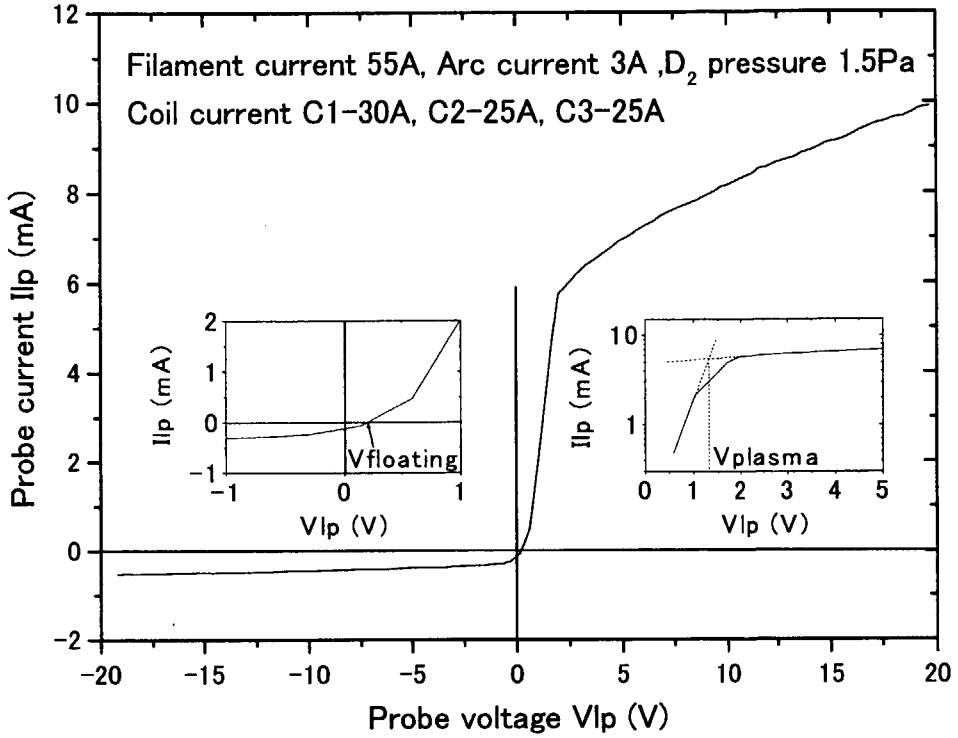

Fig. 20. Characteristic curve of the Langmuir probe recorded at position of 20 mm, also showing the plasma and the floating voltages of 1.3 and 0.2 V, respectively, in the insets.

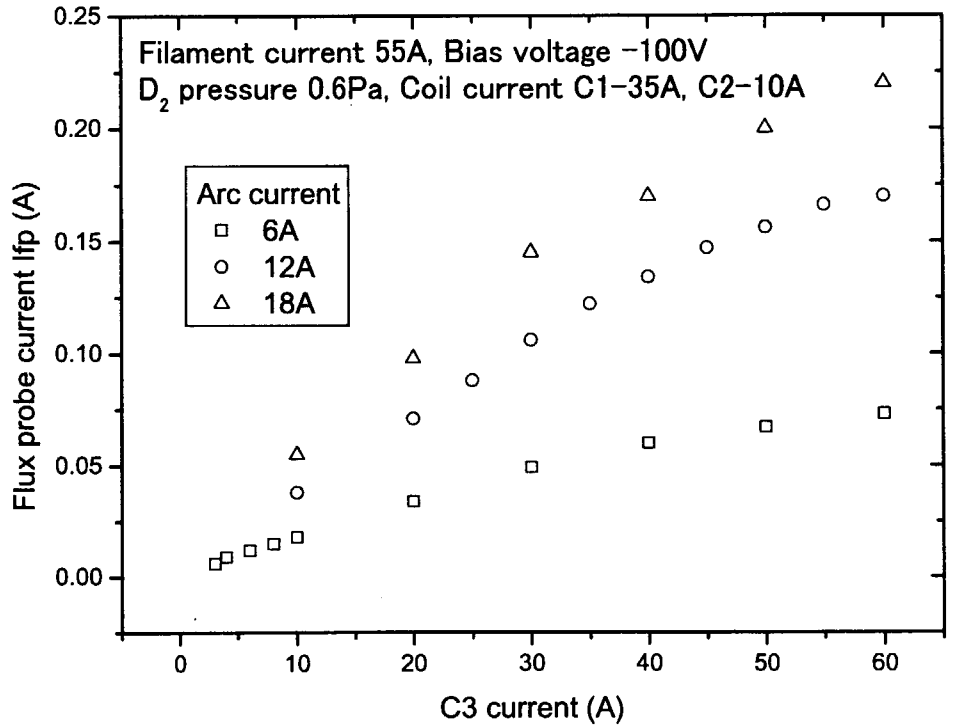

Fig. 21. C3 current dependence of flux probe current Ifp at different arc currents.

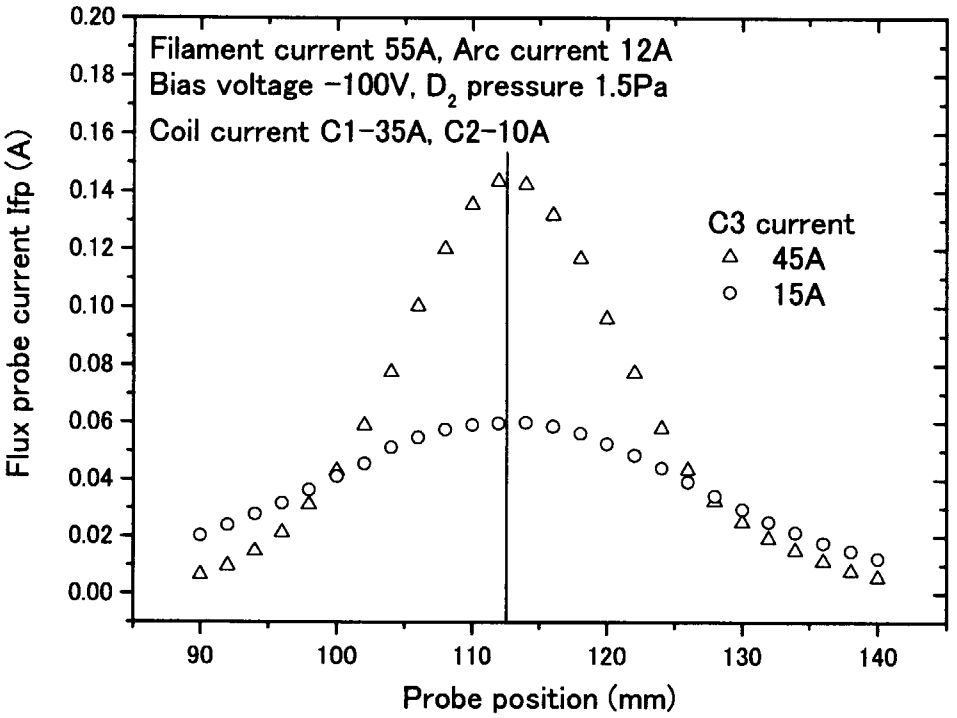

Fig. 22. Flux distribution measured with the flux probe at different C3 currents.

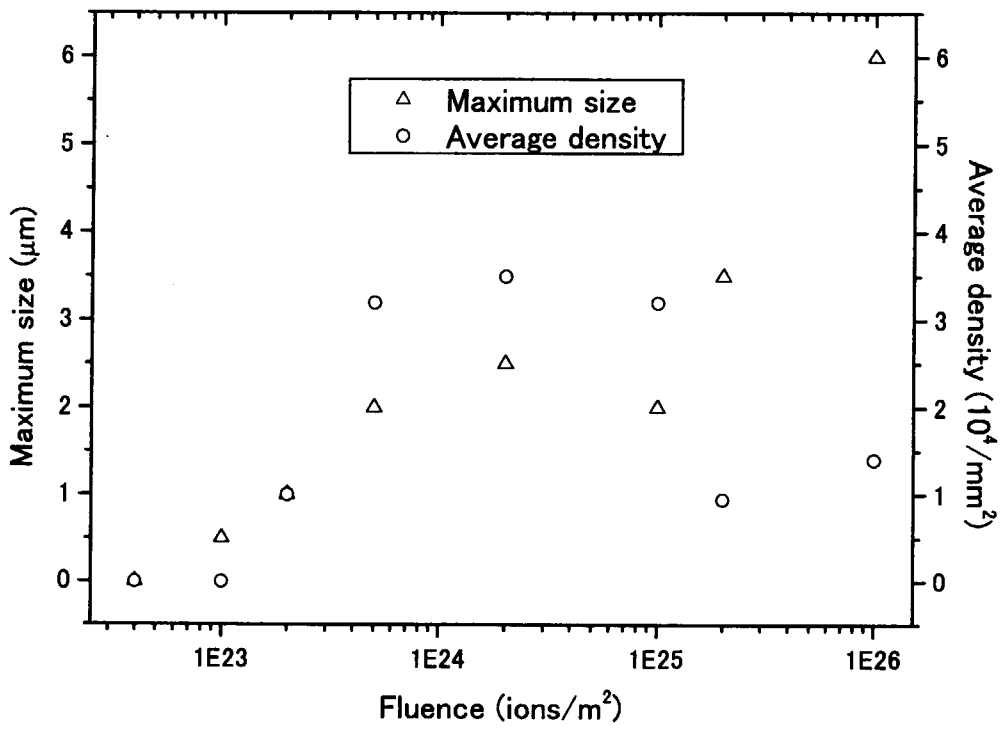

Fig. 23. Variation of maximum size and average density of blisters with irradiation fluence.

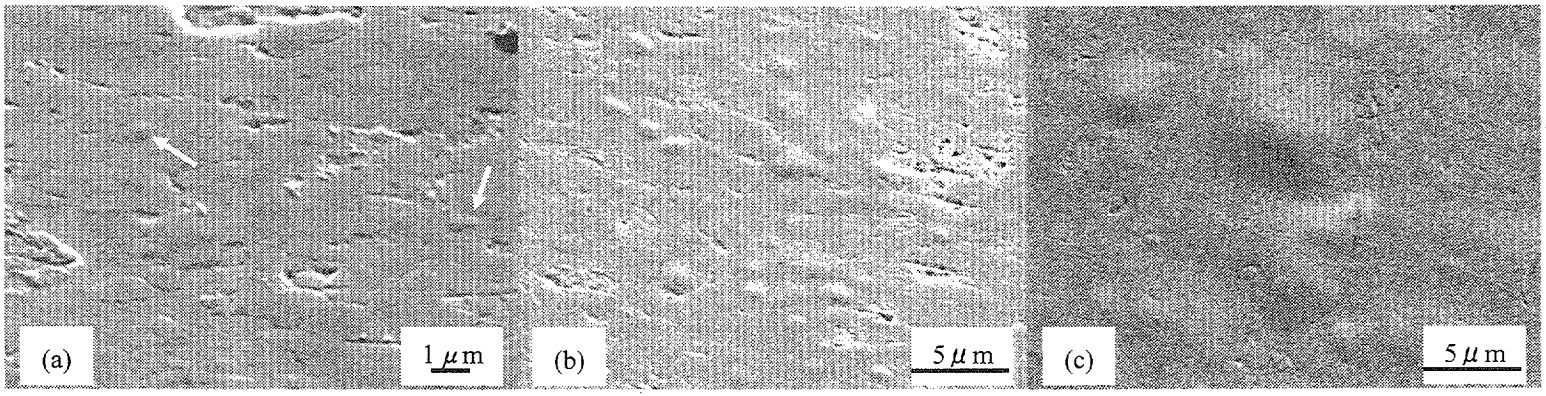

Fig. 24. (a) Small blisters as pointed by arrows occurred at the critical fluence around 1×10^{23} /m^2; (b) the maximum blister density was observed at the fluence of 2×10^{24} /m^2; (c) blister size increased monotonically to about 6 μm at the maximum fluence of 1×10^{26} /m^2 in the experiment.

This is a blank page.

国際単位系（SI）と換算表

表1　SI基本単位および補助単位

量	名称	記号
長さ	メートル	m
質量	キログラム	kg
時間	秒	s
電流	アンペア	A
熱力学温度	ケルビン	K
物質量	モル	mol
光度	カンデラ	cd
平面角	ラジアン	rad
立体角	ステラジアン	sr

表2　SIと併用される単位

名称	記号
分，時，日	min，h，d
度，分，秒	°，′，″
リットル	l，L
トン	t
電子ボルト	eV
原子質量単位	u

1 eV=1.60218×10^{-19}J

1 u=1.66054×10^{-27}kg

表3　固有の名称をもつSI組立単位

量	名称	記号	他のSI単位による表現
周波数	ヘルツ	Hz	s^{-1}
力	ニュートン	N	$m\cdot kg/s^2$
圧力，応力	パスカル	Pa	N/m^2
エネルギー，仕事，熱量	ジュール	J	N·m
工率，放射束	ワット	W	J/s
電気量，電荷	クーロン	C	A·s
電位，電圧，起電力	ボルト	V	W/A
静電容量	ファラド	F	C/V
電気抵抗	オーム	Ω	V/A
コンダクタンス	ジーメンス	S	A/V
磁束	ウェーバ	Wb	V·s
磁束密度	テスラ	T	Wb/m^2
インダクタンス	ヘンリー	H	Wb/A
セルシウス温度	セルシウス度	℃	
光束	ルーメン	lm	cd·sr
照度	ルクス	lx	lm/m^2
放射能	ベクレル	Bq	s^{-1}
吸収線量	グレイ	Gy	J/kg
線量等量	シーベルト	Sv	J/kg

表4　SIと共に暫定的に維持される単位

名称	記号
オングストローム	Å
バーン	b
バール	bar
ガル	Gal
キュリー	Ci
レントゲン	R
ラド	rad
レム	rem

1 Å=0.1nm=10^{-10}m

1 b=100fm^2=10^{-28}m^2

1 bar=0.1MPa=10^{5}Pa

1 Gal=1cm/s^2=10^{-2}m/s^2

1 Ci=3.7×10^{10}Bq

1 R=2.58×10^{-4}C/kg

1 rad=1cGy=10^{-2}Gy

1 rem=1cSv=10^{-2}Sv

表5　SI接頭語

倍数	接頭語	記号
10^{18}	エクサ	E
10^{15}	ペタ	P
10^{12}	テラ	T
10^{9}	ギガ	G
10^{6}	メガ	M
10^{3}	キロ	k
10^{2}	ヘクト	h
10^{1}	デカ	da
10^{-1}	デシ	d
10^{-2}	センチ	c
10^{-3}	ミリ	m
10^{-6}	マイクロ	μ
10^{-9}	ナノ	n
10^{-12}	ピコ	p
10^{-15}	フェムト	f
10^{-18}	アト	a

（注）

1．表1－5は「国際単位系」第5版，国際度量衡局1985年刊行による。ただし，1 eVおよび1 uの値はCODATAの1986年推奨値によった。

2．表4には海里，ノット，アール，ヘクタールも含まれているが日常の単位なのでここでは省略した。

3．barは，JISでは流体の圧力を表わす場合に限り表2のカテゴリーに分類されている。

4．EC閣僚理事会指令ではbar，barnおよび「血圧の単位」mmHgを表2のカテゴリーに入れている。

換算表

力	N(=10^{5}dyn)	kgf	lbf
	1	0.101972	0.224809
	9.80665	1	2.20462
	4.44822	0.453592	1

粘度　1 Pa·s(N·s/m^2)=10 P(ポアズ)(g/(cm·s))

動粘度　1m^2/s=10^{4}St(ストークス)(cm^2/s)

圧力	MPa(=10bar)	kgf/cm^2	atm	mmHg(Torr)	lbf/in^2(psi)
	1	10.1972	9.86923	7.50062×10^3	145.038
	0.0980665	1	0.967841	735.559	14.2233
	0.101325	1.03323	1	760	14.6959
	1.33322×10^{-4}	1.35951×10^{-3}	1.31579×10^{-3}	1	1.93368×10^{-2}
	6.89476×10^{-3}	7.03070×10^{-2}	6.80460×10^{-2}	51.7149	1

エネルギー・仕事・熱量	J(=10^7 erg)	kgf·m	kW·h	cal(計量法)	Btu	ft·lbf	eV
	1	0.101972	2.77778×10^{-7}	0.238889	9.47813×10^{-4}	0.737562	6.24150×10^{18}
	9.80665	1	2.72407×10^{-6}	2.34270	9.29487×10^{-3}	7.23301	6.12082×10^{19}
	3.6×10^6	3.67098×10^5	1	8.59999×10^5	3412.13	2.65522×10^6	2.24694×10^{25}
	4.18605	0.426858	1.16279×10^{-6}	1	3.96759×10^{-3}	3.08747	2.61272×10^{19}
	1055.06	107.586	2.93072×10^{-4}	252.042	1	778.172	6.58515×10^{21}
	1.35582	0.138255	3.76616×10^{-7}	0.323890	1.28506×10^{-3}	1	8.46233×10^{18}
	1.60218×10^{-19}	1.63377×10^{-20}	4.45050×10^{-26}	3.82743×10^{-20}	1.51857×10^{-22}	1.18171×10^{-19}	1

1 cal= 4.18605J（計量法）

= 4.184J（熱化学）

= 4.1855J（15℃）

= 4.1868J（国際蒸気表）

仕事率　1 PS(仏馬力)

= 75 kgf·m/s

= 735.499W

放射能	Bq	Ci
	1	2.70270×10^{-11}
	3.7×10^{10}	1

吸収線量	Gy	rad
	1	100
	0.01	1

照射線量	C/kg	R
	1	3876
	2.58×10^{-4}	1

線量当量	Sv	rem
	1	100
	0.01	1

（86年12月26日現在）

Characteristics of a Low Energy and High Flux Compact Plasma Source and Preliminary Results in Studying Surface Modification of Tungsten Irradiated by the Source

R100
古紙配合率100%再生紙を使用しています